Bull. Mater. Sci., Vol. 16, No. 1, February 1993, pp. 1–17. © Printed in India.

Mechanical alloying—a novel synthesis route for amorphous phases

B S MURTY
Department of Metallurgy, Indian Institute of Science, Bangalore 560012, India

MS received 2 June 1992

Abstract. Mechanical alloying (MA) pioneered by Benjamin is a technique for the extension of solid solubility in systems where the equilibrium solid solubility is limited. This technique has, in recent years, emerged as a novel alternate route for rapid solidification processing (RSP) for the production of metastable crystalline, quasicrystalline, amorphous phases and nanocrystalline materials. The glass-forming composition range (GFR), in general, is found to be much wider in case of MA in comparison with RSP. The amorphous powders produced by MA can be compacted to bulk shapes and sizes and can be used as precursors to obtain high strength materials. This paper reports the work done on solid state amorphization by MA in Ti–Ni–Cu and Al–Ti systems where a wide GFR has been obtained. Al–Ti is a classic case where no glass formation has been observed by RSP, while a GFR of 25–90 at. % Ti has been obtained in this system, thus demonstrating the superiority of MA over RSP. The free energy calculations made to explain GFR are also presented.

Keywords. Mechanical alloying; solid state amorphization; glass forming composition range; free energy-composition diagrams.

1. Introduction

The pioneering work of Benjamin in the late sixties has led to the development of a solid state processing technique, widely known as mechanical alloying (MA) (Benjamin 1976; Gilman and Benjamin 1983). This process involves milling of pure metal mixtures in high energy ball mills. During high energy ball milling, repeated welding, fracturing and rewelding of powder particles takes place which results in the formation of highly deformed particles containing alternate layers of different constituents of the original elemental blend. These fine-layered structures aided by deformation-induced-defects enhance the diffusion rates and thus result in alloying. This technique was originally developed to produce oxide dispersion strengthened (ODS) Ni and Fe base superalloys and Al alloys which were found to be much superior in their high temperature strength when compared to cast and wrought superalloys and SAP alloys respectively (Sundaresan and Froes 1987). It has been shown by several investigators that MA can be effectively used to synthesize all the metastable structures that are possible by rapid solidification processing (RSP), viz. extension of terminal solid solubility (Uenishi *et al* 1991), metastable crystalline (Fecht *et al* 1990), quasicrystalline (Eckert *et al* 1991) and amorphous (Koch *et al* 1983) phases. In addition MA has resulted in the synthesis of nanocrystalline structures (Oehring and Bormann 1991) and extension of solid solubility in the liquid immiscible systems (Suryanarayana and Froes 1991) which are difficult to be achieved by RSP.

Amorphous phase formation is the most widely studied (Johnson 1986; Weeber and Bakker 1988; Koch 1989) aspect of MA as it is the simplest of all solid state amorphization (SSA) techniques. The main advantage of MA over RSP with regard to amorphization is that the glass-forming composition range (GFR), in general, is much wider in the former case. In the case of RSP, GFR is restricted mainly to the

deep eutectic regions due to kinetic constraints. Also glass formation is very difficult by RSP for the compositions corresponding to stable intermetallic compounds and in liquid immiscible systems. However, amorphization of intermetallic compounds (Schwarz and Koch 1986), mixture of intermetallic compounds (Lee *et al* 1988) and liquid immiscible alloys (Veltl *et al* 1991) has been achieved by MA. Amorphization is also difficult by RSP in systems with shallow eutectics and cascade of peritectics. Recently, El-Eskandarany *et al* (1990) have shown a GFR of 10–90 at.% Ta by MA in Al–Ta system, wherein amorphization has not been observed so far by RSP. Incidentally, this is the widest GFR obtained in a binary alloy system by MA. The present paper reports work done by the author on a similar system, Al–Ti, in which no glass formation has been obtained by RSP. Earlier Schultz (1988) reported a GFR of 35–55 at.% Ti in this system without mentioning about the mill and milling conditions used. Cocco *et al* (1990) and Bonetti *et al* (1990) also observed the amorphization of $Al_{25}Ti_{75}$ in a Spex mill but they could not amorphize $Al_{75}Ti_{25}$ in their study. Very recently, Guo *et al* (1991) reported the formation of amorphous phase over a composition range of 50–80 at.% Ti by MA. But the present author has obtained a much wider GFR of 25–90 at.% Ti in this system by MA in a planetary mill.

Even though amorphization has been reported in many binary alloy systems by MA, reports on ternary alloy systems are very few (Matsuki *et al* 1988; Sundaresan *et al* 1988; Murty *et al* 1990). With wide GFRs observed in binary Ti–Ni (Schwarz *et al* 1985) and Ti–Cu (Politis and Johnson 1986) systems, the ternary Ti–Ni–Cu system has been chosen for the present study. Sundaresan *et al* (1988) were the first to report amorphous phase formation in Ti–Ni–Cu system for the elemental blend of composition $Ti_{72}Ni_{16}Cu_{12}$ using a Spex Mill. Subsequently, Murty *et al* (1990) reported amorphous phase formation for the compositions $Ti_{60}Ni_{40-x}Cu_x$ ($x = 10$, 20, 30) in this system in a planetary mill. This paper reports a much wider GFR in this system.

In recent years, free energy-composition and enthalpy-composition diagrams are being widely used to assess GFR in binary alloy systems (Van der Kolk *et al* 1988). Gallego *et al* (1990) recently extended this approach to ternary alloy systems by neglecting the ternary interaction parameters. Murty *et al* (1992) have shown a wide GFR towards the Ni rich side of Ti–Ni–Cu system using this approach. The GFR obtained by these thermodynamic calculations are compared with the experimental GFR obtained in Al–Ti and Ti–Ni–Cu systems by MA.

2. Experimental

Pure metal powders of −325 mesh (45×10^3 nm) have been thoroughly mixed to get $Al_{100-x}Ti_x$ ($x = 10, 20, 30, 40, 50, 60, 70, 80, 90$) compositions in the case of Al–Ti system and $Ti_{40}Ni_{60-x}Cu_x$ ($x = 10, 20, 30, 40, 50$), $Ti_{50}Ni_{50-x}Cu_x$ ($x = 10, 15, 20, 25, 30, 35, 40$) and $Ti_{60}Ni_{40-x}Cu_x$ ($x = 10, 20, 30$) in the case of Ti–Ni–Cu system. These elemental blends were mechanically alloyed in Fritsch Pulverisette-7, a microplanetary mill. The milling was carried out in wet condition in WC vial with WC balls of 15 mm diam with a ball-to-powder weight ratio of 10:1. A milling intensity of 6 was used for all samples except for $Al_{75}Ti_{25}$ where it was increased to 9 to study the effect of milling intensity on the glass forming ability. The milling intensity 6 corresponds to 490 rpm or to a ball velocity of $4{\cdot}6\,ms^{-1}$ or to a kinetic energy of 0·27 J per ball,

whereas the intensity 9 is equivalent to 645 rpm or to a ball velocity of 6·1 ms^{-1} or to a kinetic energy of 0·47 J per ball. The maximum bulk temperature rise of the powder was observed to be 25 K at a milling intensity 6 and 35 K at milling intensity 9.

The powder samples at different intervals of milling were characterized by X-ray diffraction (XRD) using Huber X-ray diffractometer with CuKα ($\lambda = 0{\cdot}15405$ nm) radiation for Ti–Ni–Cu alloys and MoKα ($\lambda = 0{\cdot}07092$ nm) radiation for Al–Ti alloys. Electron microscopy was done using JEOL scanning electron microscope (SEM) and Phillips 100 kV transmission electron microscope (TEM). Crystallization studies were carried out using Perkin–Elmer differential scanning calorimeter (DSC-2C) at a heating rate of 40 K min^{-1}.

3. Results

3.1 *Al–Ti system*

XRD patterns of $Al_{50}Ti_{50}$ samples after different durations of MA are shown in figure 1. With increasing milling time the Ti and Al peaks became broader and less intense. The peak broadening was used to calculate the effective particle size (L) using Scherrer's formula

$$L = 0{\cdot}9\lambda/\beta \cos\theta, \tag{1}$$

where λ is the wavelength of radiation, β, the full width at half maximum in radians and θ, the Bragg angle. The effective particle sizes of Al and Ti decreased more rapidly during the first 8 h of milling, reaching a value around 15 nm from an initial value of 45×10^3 nm and further milling resulted in a marginal decrease. A broad peak corresponding to the amorphous phase started appearing after 16 h of MA. Further

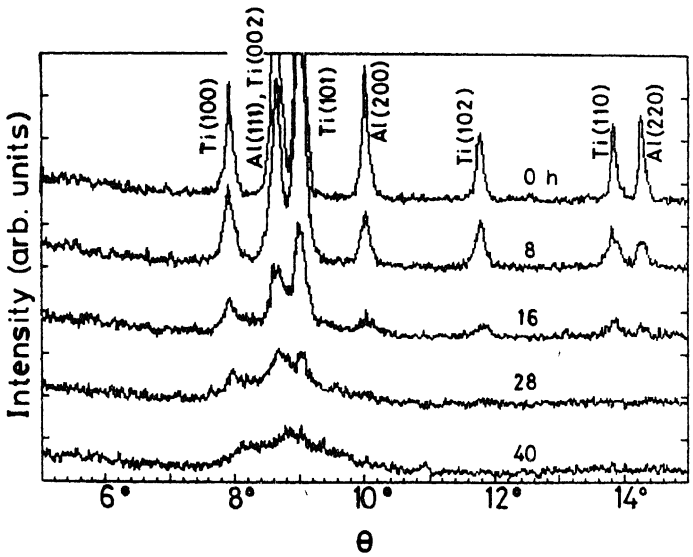

Figure 1. XRD patterns of $Al_{50}Ti_{50}$ with different durations of MA at a milling intensity of 6.

milling resulted in the disappearance of pure metal crystalline peaks and the amorphization reaction was found to be complete after 40 h of MA. The wavenumber corresponding to the amorphous broad peak was 26·4 nm^{-1}, which compared well with that observed by Schultz (1988) and Cocco *et al* (1990).

After 40 h of milling compositions corresponding to 40–90 at.% Ti were found to be amorphous, whereas, Al-rich compositions remained crystalline. The wavenumber of the amorphous broad peak decreased from 26·5 to 25·9 nm^{-1} with increasing Ti content from 40–90 at.% in the alloy. This variation of the amorphous peak with composition was marginal when compared to that observed in an earlier study by the authors for Ti–Ni system (Murty *et al* 1992), where the wavenumber varied from 27·6 to 30·8 nm^{-1} in the composition range 10–70 at.% Ni. The relative insensitivity of the wavenumber of the amorphous broad peak to the composition in Al–Ti system was expected as the metallic radii of Ti and Al were very similar (0·147 and 0·143 nm respectively). In the case of Ti–Ni system, as the metallic radii of Ti and Ni (0·147 and 0·128 nm respectively), were significantly different, the variation of wavenumber of amorphous peak with composition was larger.

In the case of Al-rich compositions the peak shifted after MA were used to get an idea about the extension of solid solubility of Ti in Al. Under equilibrium conditions the solid solubility of Ti in Al was negligible at room temperature (Willey and Margolin 1973). Pearson (1974) reported that the lattice parameter of Al decreased by 0·001 nm for 1 at.% of Ti in solution in the solid state. From the change in the lattice parameter of Al after 40 h of MA the solubility of Ti in case of $Al_{100-x}Ti_x$ ($x = 70, 80, 90$) samples was found to be only 0·4 at.%. In case of $Al_{75}Ti_{25}$ which was milled at 645 rpm after 20 h of MA itself the solubility of Ti in Al was found to be 4 at.% which was much higher than the equilibrium solubility. This was 1 at.% higher than the extension of solubility obtained by Cocco *et al* (1990) for the same composition after 21 h of milling in a Spex mill. It is interesting to note that the maximum solid solubility of Ti in Al obtained by RSP was only 2 at.% (Hori *et al* 1985). The amorphous peak

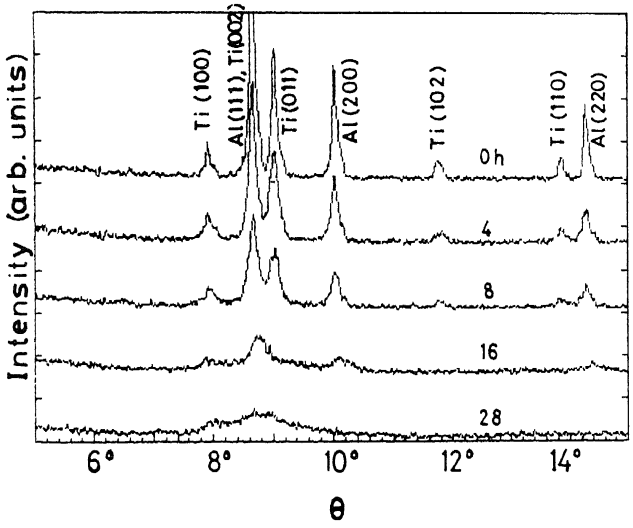

Figure 2. XRD patterns of $Al_{75}Ti_{25}$ as a function of duration of MA showing the evolution of amorphous phase at a milling intensity of 9.

started appearing after 10 h of MA and finally after 28 h of milling, this sample was transformed completely into an amorphous phase as shown in figure 2.

The formation of alternate layers of Al and Ti in MA powders was observed in SEM study. Figures 3a and 3b show the secondary electron image and back scattered image respectively, of a powder particle corresponding to the $Al_{50}Ti_{50}$ sample. The composition contrast in the back scattered image clearly indicated the presence of alternate layers of Al and Ti in the powder particle. The formation of amorphous phase was confirmed by TEM. Figures 4a–d show the selected area diffraction patterns of $Al_{50}Ti_{50}$ sample after 4, 8, 16 and 40 h of MA respectively. The destabilization of the crystal structure with increasing milling time was clearly evident from the heavy

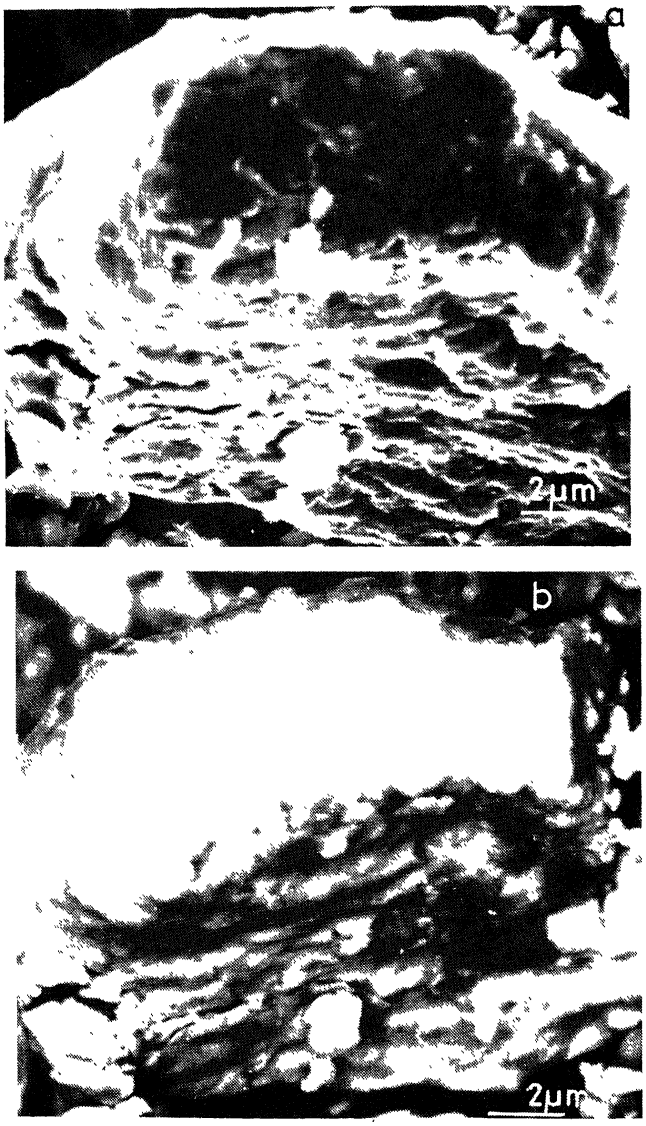

Figure 3. SEM micrograph of a powder particle from $Al_{50}Ti_{50}$ sample after 4 h of MA. (**a**) Secondary electron image and (**b**) back scattered image.

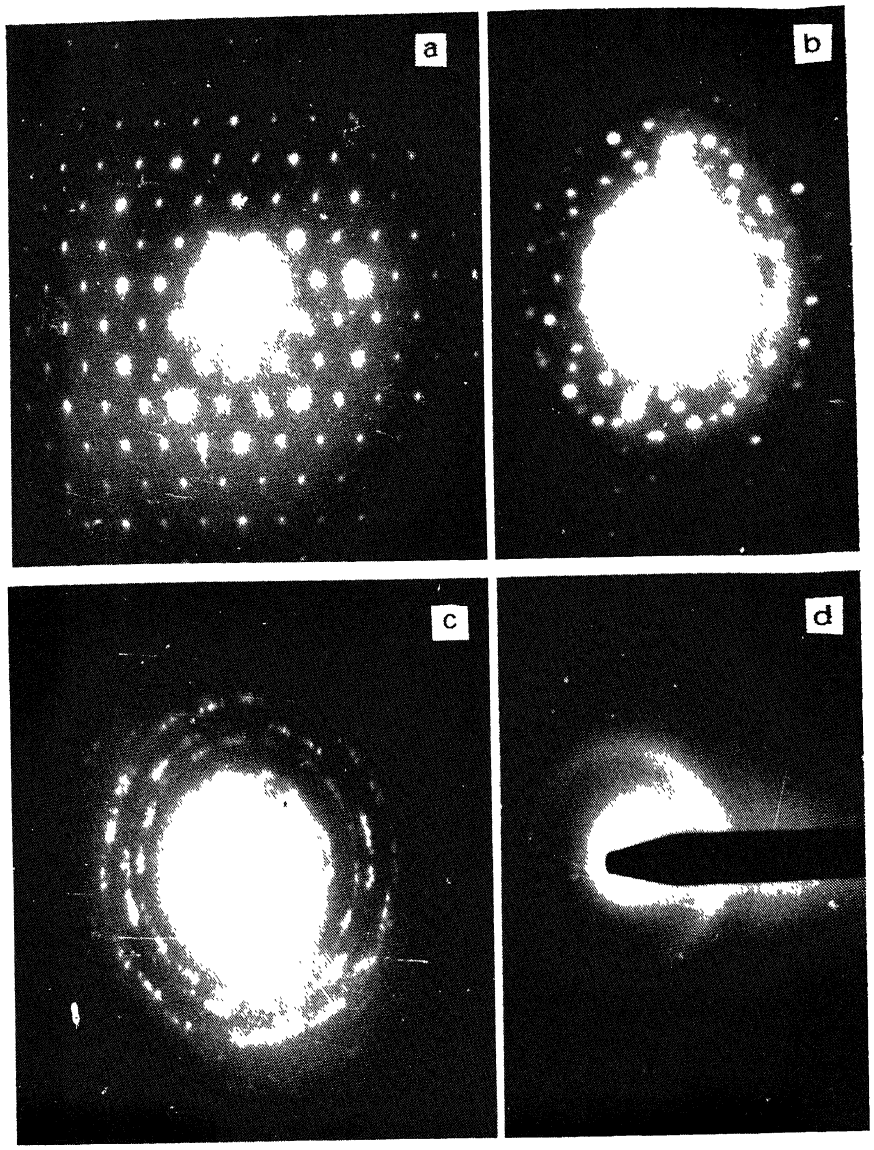

Figure 4. TEM selected area diffraction patterns of $Al_{50}Ti_{50}$ after (**a**) 4 h, (**b**) 8 h, (**c**) 16 h and (**d**) 40 h of MA.

twinning and streaking of the spots indicating distortion of the lattice (figures 4b and c). Further milling of the sample resulted in complete amorphization after 40 h as shown in figure 4d. Similar results were obtained in other alloys and samples in the composition range of 40–90 at%. Al have shown an amorphous nature after 40 h of MA at a milling intensity 6. The sample $Al_{75}Ti_{25}$ which was milled at intensity 9 became amorphous within 28 h of MA.

3.2 *Ti–Ni–Cu system*

A GFR of 10–70 at.% Ni in Ti–Ni system and 10–50 at.% Cu in Ti–Cu system was obtained in the present study by MA at milling intensity 6. Figure 5 shows XRD

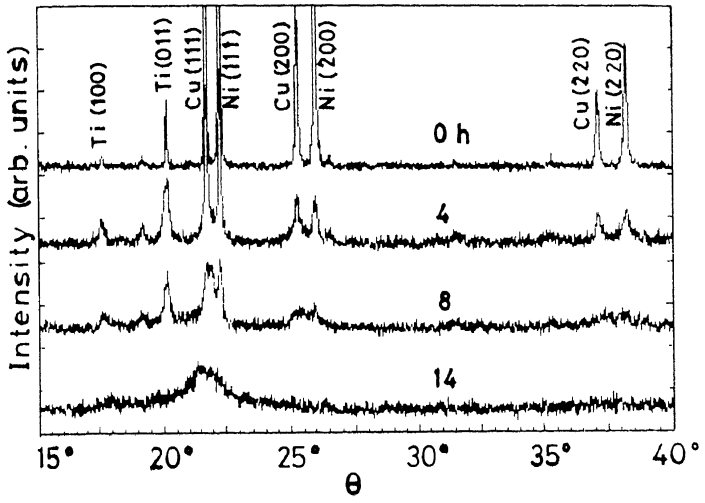

Figure 5. XRD patterns of $Ti_{40}Ni_{30}Cu_{30}$ as a function of duration of showing the evolution of amorphous phase.

patterns of mechanically alloyed powders of the composition $Ti_{40}Ni_{30}Cu_{30}$ as a function of milling time. The XRD pattern of elemental blend showed the most intense peaks of Ti, Ni and Cu which became more and more broad and their intensity decreased as milling proceeded. After 12 h of milling it was observed that both Ni(111) and Cu(111) peaks disappear and a broad peak corresponding to the amorphous phase appear. After milling for 14 h the last traces of Ti(011) peak also disappeared and the alloy became completely amorphous. The maximum of this amorphous peak was at 29·9 nm^{-1}.

The XRD results of all 15 compositions after 40 h of MA are shown (table 1). It was observed that the middle compositions in the three groups of alloy compositions studied, viz. $Ti_{60}Ni_{20}Cu_{20}$, $Ti_{50}Ni_{25}Cu_{25}$ and $Ti_{40}Ni_{30}Cu_{30}$ became amorphous within 14 h indicating their faster rate of amorphization. When the milling was prolonged to 40 h crystallinity remained in the Cu-rich compositions, viz. $Ti_{50}Ni_{50-x}Cu_x$ ($x = 35, 40$) and $Ti_{40}Ni_{10}Cu_{50}$. The composition $Ti_{60}Ni_{10}Cu_{30}$ was partially amorphous after 40 h of MA.

TEM was used to confirm amorphization in all the cases where amorphous broad peak was observed by XRD. Figure 6 shows GFR obtained by MA in the present study along with typical selected area electron diffraction patterns of amorphous, amorphous + crystalline and crystalline phases.

DSC studies carried out on the mechanically alloyed powders have shown some interesting results. The DSC results obtained at 40 K min^{-1} are presented in table 1. The DSC traces of two representative compositions studied at this heating rate are shown in figure 7. Two important features were clearly evident from figure 7 and table 1. Firstly, the crystallization temperature T_x, was maximum at the middle composition for all the three groups of alloy compositions studied. The fact that the rate of amorphization was also the fastest for these three compositions indicated that the amorphous phase formation was more favourable and that they were more stable at these compositions. Secondly, in the case of Cu-rich elemental blends, where complete amorphization was not observed even after 40 h of MA, the crystallization peak was preceded by another exothermic peak.

Table 1. XRD and DSC results of Ti–Ni–Cu samples.

Composition	Milling time for amorphization (h)	Amorphization peak (K)	Crystallization peak (K)
$Ti_{60}Ni_{30}Cu_{10}$	40	—	574
$Ti_{60}Ni_{20}Cu_{20}$	14	—	616
$Ti_{60}Ni_{10}Cu_{30}$	Partial amorphization after 40 h	482	554
$Ti_{50}Ni_{40}Cu_{10}$	18	—	598
$Ti_{50}Ni_{35}Cu_{15}$	18	—	616
$Ti_{50}Ni_{30}Cu_{20}$	18	—	620
$Ti_{50}Ni_{25}Cu_{25}$	14	—	630
$Ti_{50}Ni_{20}Cu_{30}$	40	—	590
$Ti_{50}Ni_{15}Cu_{35}$	No amorphization even after 40 h	486	584
$Ti_{50}Ni_{10}Cu_{40}$	No amorphization even after 40 h	496	580
$Ti_{40}Ni_{50}Cu_{10}$	18	—	618
$Ti_{40}Ni_{40}Cu_{20}$	18	—	624
$Ti_{40}Ni_{30}Cu_{30}$	14	—	638
$Ti_{40}Ni_{20}Cu_{40}$	40	—	620
$Ti_{40}Ni_{10}Cu_{50}$	No amorphization even after 40 h	512	598

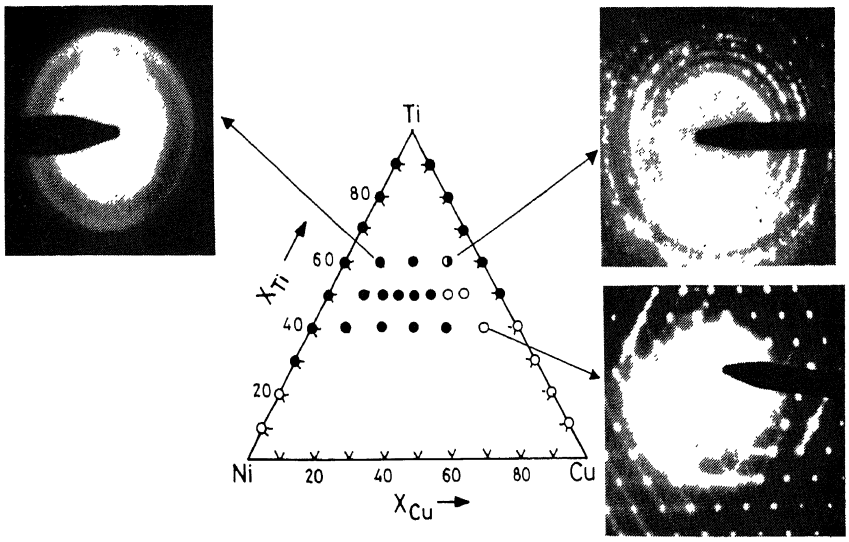

Figure 6. The experimental GFR by MA after 40 h of MA along with typical selected area electron diffraction patterns. (○ crystalline, ◑ amorphous + crystalline and ● amorphous).

Recently, Schulz *et al* (1991) reported three exothermic peaks for the mechanically alloyed $NiZr_2$ samples. They attributed the first exothermic peak to thermally-induced SSA, the second to structural recovery and recrystallization of the crystalline powder mixture and the third to the crystallization of the amorphous phase. In the present study, samples quenched in DSC from the first exothermic peak have revealed their

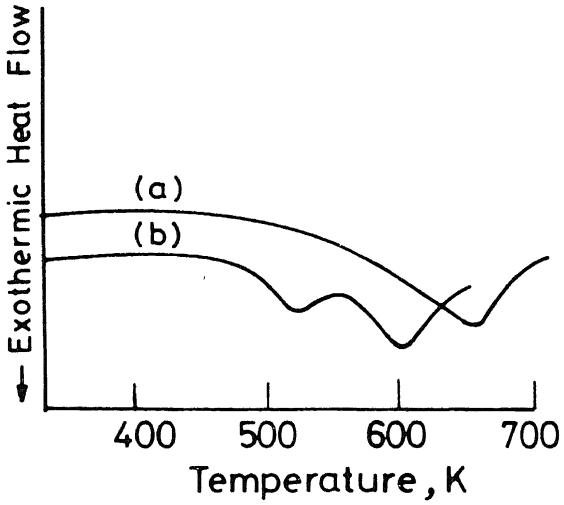

Figure 7. DSC traces of (a) $Ti_{40}Ni_{30}Cu_{30}$ after 14 h of milling and (b) $Ti_{40}Ni_{10}Cu_{50}$ after 40 h of milling, at a heating rate of 40 K/min.

amorphous nature in TEM study. Thus the first exothermic peak observed in the present study was attributed to the thermally-induced amorphization. However, we cannot preclude the possibility of structural recovery and recrystallization of the remaining crystalline powder particles occurring simultaneously. This amorphous phase which was formed at lower temperature in DSC in turn crystallized at higher temperature giving rise to a second exothermic peak. This has also been observed by Highmore *et al* (1987) in multilayer diffusion couple experiments. In cases where the alloy was already amorphous, only a crystallization peak was observed.

4. Discussion

4.1 *Al–Ti system*

The fact that $Al_{75}Ti_{25}$ which was outside GFR at milling intensity 6, amorphized within 28 h of milling at the milling intensity 9, indicating that GFR is wider at a higher milling speed. This was not unexpected because at higher milling speeds the energy of impact of the ball with the powder was found to be higher which in turn resulted in production of more number of defects in the crystalline pure metal mixture. The rms strain can be used as a measure of lattice strain which can be calculated from the XRD data, using the following equation (Friedel 1964).

$$\Delta K = A\langle e^2\rangle^{1/2} K, \tag{2}$$

where K is the wave vector corresponding to any XRD peak, ΔK, the full width at half maximum, $\langle e^2\rangle^{1/2}$, the rms strain and A, a constant which depended on strain distribution. This coefficient is approximately unity for random distribution of dislocations (Atzmon *et al* 1985).

Figures 8a and b show the rms strain calculated using the above equation for Al and Ti as a function of milling time for $Al_{50}Ti_{50}$ milled at intensity 6 and $Al_{75}Ti_{25}$

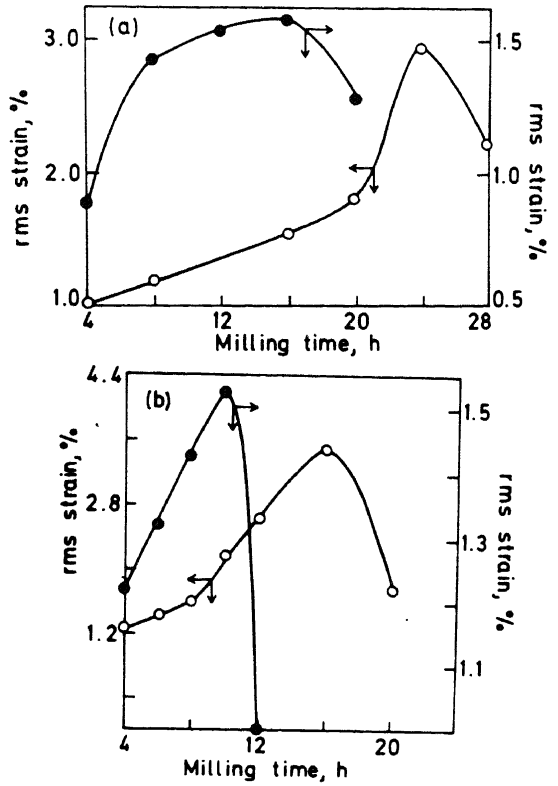

Figure 8. The rms strain in Al (○) and Ti (●) crystals in (**a**) $Al_{50}Ti_{50}$ and (**b**) $Al_{75}Ti_{25}$ as a function of milling time. The left hand side scale refers to Al and the right hand side scale refers to Ti.

milled at intensity 9 respectively. The full width at half maximum intensity of the Al(111) and Ti(011) peaks has been used for this calculation. For $Al_{50}Ti_{50}$ the strain in Ti reached a maximum at 16 h (figure 8a) when the XRD pattern showed the appearance of an amorphous phase. Similarly, for $Al_{75}Ti_{25}$ alloy also the strain in Ti reached a maximum (figure 8b) when the amorphous started forming, which occurred at 10 h. This supports the earlier reports (Schwarz and Koch 1986; Schulz *et al* 1991) that the amorphization starts when the strain in the crystal, especially the relatively non-diffusing metal, reaches a critical value. This critical strain enhances the diffusion rates and aids in destabilizing the crystal and nucleation of the amorphous phase.

The strain in Al reached a maximum after the amorphous phases started forming (figures 8a and b) indicating that it was the strain in the non-diffusing Ti that played a more important role. The strain in Al after 16 h of milling in the case of $Al_{75}Ti_{25}$ was twice that of $Al_{50}Ti_{50}$ which points out that the higher milling speeds indeed result in large strains in the lattice. But, this was not observed in the case of Ti which again proves the hypothesis that the amorphous phase starts forming when the strain in the non-diffusing element reaches a critical value independent of the milling conditions. The formation of an amorphous phase results in the relaxation which decreases the strain. This explains the fall in the strain after it has reached a critical value.

It is in general accepted that two criteria should be fulfilled by any binary system for SSA (Schwarz and Johnson 1983). First, the heat of mixing in the amorphous phase, which is assumed to be the supercooled liquid for most of the thermodynamic calculations, should be more negative when compared to that of crystalline solid solution thus providing a chemical driving force for its formation. Secondly, the diffusivity of one element in the other should be anomalously fast so that nucleation and growth of more stable intermetallic compounds is kinetically constrained. The second criterion seems to be satisfied in the case of Al–Ti system. Calculation of diffusivities from the standard data (Smithells 1983) has shown that the self diffusivity of Al and α–Ti at the operating temperature of about 300 K is $2{\cdot}9 \times 10^{-25}$ and $6{\cdot}0 \times 10^{-32} \mathrm{cm^2 s^{-1}}$ respectively. The chemical diffusivity of Al in α–Ti at this temperature was $8{\cdot}7 \times 10^{-23} \mathrm{cm^2 s^{-1}}$ which is around nine orders higher than that of the self diffusivity of α–Ti.

In order to find out the existence of any driving force for the formation of amorphous phase, thermodynamic calculations were carried out. Two approaches were chosen for calculation, one based on the CALPHAD approach with the regular solution model and the other being the Miedema's enthalpy calculation approach.

In the regular solution model the free energy of any phase, i, is given by,

$$G^i = x_A G^i_A + x_B G^i_B + x_A x_B \Omega^i + \mathrm{RT}(x_A \ln x_A + x_B \ln x_B), \tag{3}$$

where G^i_A and G^i_B are the free energies of pure metals A and B in the form of i. Ω^i is the interaction parameter, x_A and x_B are the molar concentrations of A and B respectively. In the above equation the first two terms on the right side of the equation refer to the free energy of the pure metal mixture. The third term is the enthalpy of mixing, ΔH^{mix}, for which the regular solution model was used. In the present calculation the temperature dependence of the interaction parameter was also considered as suggested by Murray (1988). The last term refers to the contribution of configurational entropy of mixing, ΔS^{mix}, to the free energy. Using (3) the free energy of liquid, α–Al and α–Ti solid solutions were calculated at 300 K. The data required for the calculation was taken from Murray (1988) who calculated the Al–Ti phase diagram recently.

In the second approach, the enthalpy of mixing was calculated using Miedema's model (Miedema *et al* 1980). In this model the enthalpy of mixing of the solid solution was expressed as (Van der Kolk *et al* 1988)

$$\Delta H^{\mathrm{sol}} = \Delta H^c + \Delta H^e + \Delta H^s, \tag{4}$$

where the superscripts c, e and s refer to the chemical, elastic and structural contributions to the enthalpy of solid solution. The chemical contribution to the enthalpy of mixing of solid solution can be written as

$$\Delta H^c = x_A x_B [x_B \Delta h^{\mathrm{sol}}_{A \text{ in } B} + x_A \Delta h^{\mathrm{sol}}_{B \text{ in } A}], \tag{5}$$

where x_A, x_B are mole fractions of A and B components respectively. Δh^{sol} is the enthalpy of solution of one element in the other in the infinite dilution limit, which were taken from Miedema's work (Niessen *et al* 1983).

The elastic term in the enthalpy equation comes basically from the atomic size mismatch which takes the form,

$$\Delta H^e = x_A x_B [x_B \Delta h^e_{A \text{ in } B} + x_A \Delta h^e_{B \text{ in } A}] \tag{6}$$

$\Delta h^e_{i \text{ in } j}$ has been obtained using Eshelby's formalism (Eshelby 1956; Simozar and

Alonso 1984) to get

$$\Delta h^{e}_{i \text{ in } j} = \frac{2\mu_j (V_i^* - V_j^*)^2}{3V_j^* + 4\mu_j K_i V_i^*}, \tag{7}$$

where μ_j is the shear modulus of the solvent, V_i^* and V_j^* are the molar volumes of solute and solvent respectively corrected for charge transfer effects (Bakker 1985) and K_i is the compressibility of the solute.

Finally, the structural contribution to the enthalpy of solid solution, arising from the difference in the valency and crystal structure of the solute and solvent, is expected to have only a minor effect in determining the GFR when compared to the elastic energy contribution. Also it is difficult to calculate this structural contribution and so it was not considered in the present calculations.

In the case of the amorphous phase, the elastic and structural contributions to its enthalpy are absent. The enthalpy of the amorphous phase was obtained by the following equation

$$H^a = \Delta H^c + x_A H^a_A + x_B H^a_B, \tag{8}$$

where ΔH^c for the amorphous phase has been obtained by multiplying (5) by the factor, $[1 + 5(x^s_A x^s_B)^2]$, to account for the short range order observed in the amorphous phases (Weeber 1987), where x^s_A and x^s_B are given by

$$x^s_A = \frac{x_A V_A^{2/3}}{x_A V_A^{2/3} + x_B V_B^{2/3}} \quad \text{and} \quad x^s_B = 1 - x^s_A \tag{9}$$

In the present calculations crystalline pure metals were chosen to be the standard state and their enthalpy was assigned to be zero. The enthalpies of amorphous pure metals was assumed to be independent of temperature and was obtained from the following equation

$$H^a_i = \alpha T_{m,i} \tag{10}$$

where H^a_i is the enthalpy of amorphous pure metal i, $T_{m,i}$ is the melting point of pure metal i, and $\alpha = 3{\cdot}5\,\text{Jmol}^{-1}\text{K}^{-1}$.

The results of free energy calculations based on regular solution model and that of the amorphous phase calculated with the Miedema's model are shown in figure 9. It can be seen clearly that at all compositions the free energy of the liquid phase is higher than that of the solid solutions indicating the absence of any driving force for its formation. It is also evident from the figure for Miedema's model that there exists a driving force for the amorphous phase in the composition range 21–69 at.% Ti. The $Al_{75}Ti_{25}$ composition which was found to amorphize at the milling intensity 9 also falls within this range. The fact that GFR depends on the model used for the enthalpy of solutions has already been reported by the authors (Murty *et al* 1989). The GFR obtained from the free energy calculations (21–69 at.% Ti) is comparable with that reported by Cocco *et al* (1990) (23–72 at.% Ti) which was calculated at 0 K.

It is interesting to point out that as the atomic radii of the two elements are similar the elastic contribution for the enthalpy of the solid solution (0·16 kJ) was found to be very small when compared to chemical contribution (30 kJ). In fact due to this reason the Egami and Waseda (1984) criterion has not yielded any GFR for this system. This points out the fact that contribution of elastic mismatch alone is not sufficient for glass formation. The chemical contribution also has to be considered.

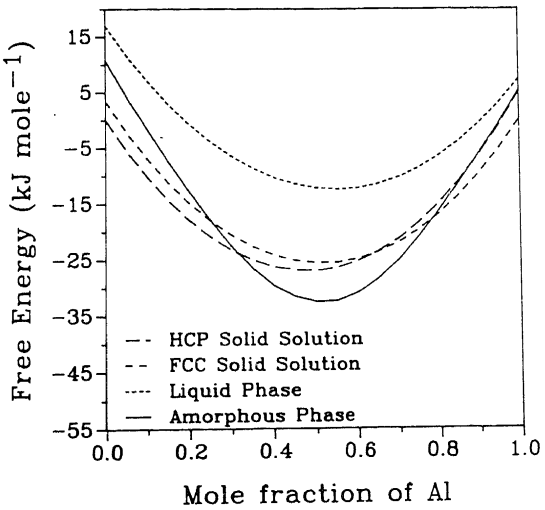

Figure 9. Free energy-composition diagram for Al–Ti system at 300 K based on regular solution model for the liquid, fcc solid solution and hcp solid solution and Miedema's for the amorphous phase.

However, in the case of Ti–Ni and Ti–Cu system, due to wide differences in the atomic radii of the elements Egami and Waseda's (1984) model predicts a GFR of 31–79 at.% Ni and 29–81 at.% Cu for Ti–Ni and Ti–Cu systems respectively.

The GFR predicted by thermodynamic calculations in this system is an underestimate when compared to that obtained by MA in the present study on the Ti rich side. Amorphization was observed even with 10 at.% Al in Ti while the free energy calculations show that a minimum concentration of 31 at.% Al is required for glass formation. This difference could be due to the fact that the energy of deformation strains and defects generated during MA has not been incorporated in the present calculations. These defects are expected to raise the free energy of solid solution thus aiding in its destabilization into an amorphous phase. But with the present understanding, the type of these defects and their concentration remains the major question. Also, the effect of milling parameters on the type and concentration of the defects is not well understood so far. These are the major blocks in quantifying the contribution of defects to the free energy of solid solution during MA. However, if this can be done one can predict GFR in any system quite accurately.

4.2 *Ti–Ni–Cu system*

In order to quantify the driving force for amorphization and to estimate the theoretical GFR, enthalpies of solid solution and amorphous phases have been calculated in this system. The reason for calculating enthalpy-composition diagrams instead of free energy-composition diagrams is that at the temperature of interest in the present study (300 K) the entropy contribution to the free energy is very small and so the driving force for amorphization comes mainly from enthalpy contribution. In the present calculations crystalline pure metals were chosen to be the standard state and their enthalpy was assigned to be zero.

The enthalpy of mixing of ternary solid solution as suggested by Gallego *et al* (1990) can be expressed as

$$\Delta H^{sol}_{ABC} = \Delta H^{c}_{ABC} + \Delta H^{e}_{ABC} + \Delta H^{s}_{ABC}, \tag{11}$$

which is similar to (4). The heat of mixing in Miedema's model (Miedema *et al* 1980) comprises a negative contribution from the electronegativity difference between the two elements and a positive contribution from the difference in electron densities of the two elements. For the present calculation this model was applied to the ternary alloy system, neglecting for a first approximation, the ternary interaction parameters. Thus the chemical contribution is given by Gallego *et al* (1990) as

$$\Delta H^{c}_{ABC} = \Delta H^{c}_{AB} + \Delta H^{c}_{BC} + \Delta H^{c}_{AC} \tag{12}$$

where ΔH^{c}_{ij} are obtained from (5). Similarly the elastic term in the enthalpy equation can be written as

$$\Delta H^{e}_{ABC} = \Delta H^{e}_{AB} + \Delta H^{e}_{BC} + \Delta H^{e}_{CA} \tag{13}$$

where ΔH^{e}_{ij} are obtained using (6) and (7).

The results obtained from these calculations have been plotted as enthalpy-composition diagrams for the three groups of alloys studied (figure 10). Each diagram shows the enthalpies of solid solution and amorphous phase vs x_{Ni} for constant x_{Ti}. The GFR obtained from these calculations was $x = 0$–30 and 58–60 for $Ti_{40}Ni_{60-x}Cu_x$,

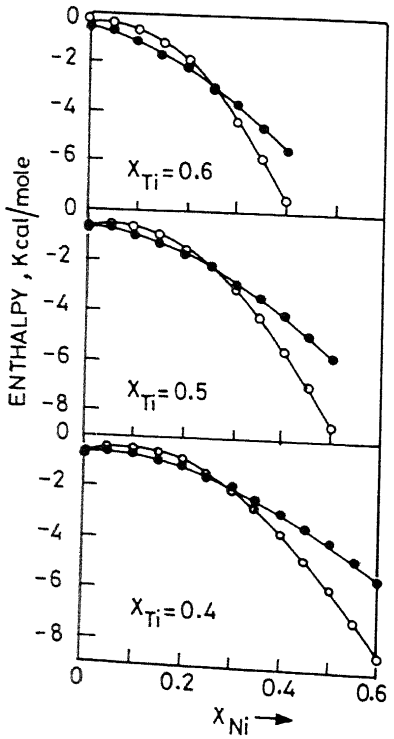

Figure 10. Enthalpy vs. x_{Ni} at constant x_{Ti} for Ti–Ni–Cu system. (○—○ amorphous phase, ●-- solid solution).

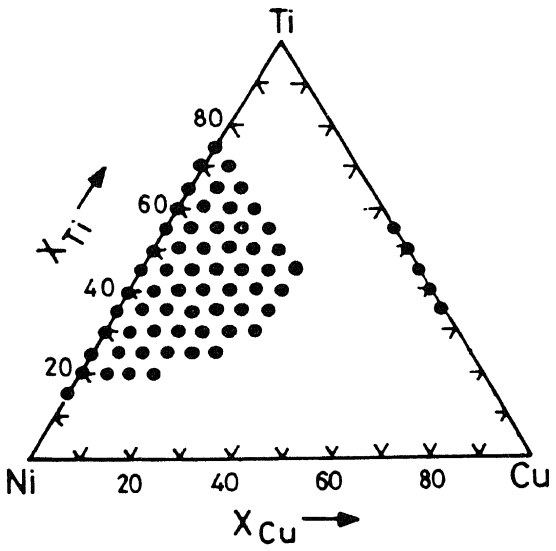

Figure 11. Theoretical GFR in Ti–Ni–Cu system. (● amorphous).

$x = 0$–24 and 49–50 for $Ti_{50}Ni_{50-x}Cu_x$ and $x = 0$–15 for $Ti_{60}Ni_{40-x}Cu_x$. The GFR obtained from these enthalpy-composition diagrams is shown in figure 11. It is interesting to note that, even though the calculated GFR does not match well with that obtained by experiment (figure 6) for the binaries, they compare fairly well in the case of ternary Ti–Ni–Cu system. The difficulty in amorphizing the Cu-rich compositions in both binary and ternary systems could be explained through the present calculations. Even the earlier calculations on T_0 curves by Schwarz *et al* (1987) and Massalski and Woychik (1985) in binary Ti–Cu system have also proved that it is very difficult to amorphize these alloys. The equilibrium phase diagram of Ti–Cu shows a number of peritectics when compared to Ti–Ni system where there are many eutectics. This also points out the fact that the enthalpy of mixing for the liquid is less negative in the former case, indicating a lower driving force for amorphization.

It is interesting to note that while the experiments show that the rate of amorphization is fastest for the middle compositions in all the three groups, enthalpy calculations show that these compositions have little or no driving force for amorphization. Also the Ni-rich compositions which exhibit substantially larger driving force take more time for amorphization. This clearly indicates that the rate of amorphization may not be directly related to the chemical driving force for amorphization as was reported earlier (Lee and Koch 1987). Further study is required in order to understand the factors controlling the rate of amorphization.

The enthalpy calculations do not show any driving force for amorphization for the Cu-rich compositions, but prolonged MA has resulted in the amorphization of some of these compositions. This could be due to the defects created during high energy milling which raise the enthalpy of the solid solution and thus provide the necessary driving force for amorphization. The present calculations do not consider this contribution.

The results indicate that the activation energy for amorphization is possibly a minimum for the middle compositions and is more on both higher Ni and Cu sides.

This results in longer milling time for amorphization on Ni-rich side even though there exists a driving force for amorphization for these compositions. On the Cu-rich side the energy supplied through milling has to be used both for providing driving force for amorphization by raising the enthalpy of the solid solution due to the introduction of defects and also to overcome the activation barrier for amorphization. In the case of those compositions which could not be amorphized even after 40 h of MA it is evident that the energy supplied by milling was insufficient to overcome the activation barrier for amorphization. This activation barrier is mainly for the diffusion of the elements and heating in DSC enhances the diffusion resulting in amorphization. As reported earlier by the authors (Murty *et al* 1990) the concept of fast diffusion should be used cautiously in ternary systems as the presence of a third element affects the rate of diffusion of one element in the other.

5. Conclusions

5.1 *Al–Ti system*

(i) The GFR in Al–Ti system has been found to be from 40–90 at.% Ti by MA at a milling intensity of 6 (490 rpm).
(ii) Use of higher milling intensity of 9 (645 rpm) has resulted in a wider GFR of 25–90 at.% Ti.
(iii) The regular solution model for free energy calculations has not shown a driving force for the amorphous phase formation at any composition in this system.
(iv) The free energy calculations based on the Miedema's formalism for the amorphous phase and CALPHAD approach for the liquid and solid solutions have shown a GFR of 21–69 at.% Ti.
(v) The amorphization was found to start when the strain in Ti, the relatively non-diffusing species, reaches a maximum value.

5.2 *Ti–Ni–Cu system*

(i) The GFR in Ti–Ni–Cu system was found to be $x = 10$–20 for $Ti_{60}Ni_{40-x}Cu_x$, $x = 10$–30 for $Ti_{50}Ni_{50-x}Cu_x$ and $x = 10$–40 for $Ti_{40}Ni_{60-x}Cu_x$ alloys.
(ii) The rate of amorphization and the thermal stability of amorphous phase were observed to be a maximum for the middle compositions in each of the three groups of ternary alloy compositions studied.
(iii) Cu-rich compositions were difficult to amorphize.
(iv) The GFR obtained from the calculated enthalpy-composition diagrams is in general agreement with the one observed experimentally.
(v) This study has indicated that the driving force for amorphization has no bearing on the rate of amorphization by MA.

Acknowledgements

The author is grateful to Professors S Ranganathan and M Mohan Rao for invaluable guidance in carrying out this work. The author is thankful to Mr Dinesh Naik for

experimental help and to the Materials and Processes Panel of the Aeronautical Research and Development Board for financial assistance.

References

Atzmon M, Unruh K M and Johnson W L 1985 *J. Appl. Phys.* **58** 3865
Bakker H 1985 *J. Less Common Metals* **105** 129
Benjamin J S 1976 *Sci. Am.* **234** 40
Bonetti E, Cocco G, Enzo S and Valde G 1990 *Mater. Sci. Tech.* **6** 1258
Cocco G, Soletta I, Battezzati L, Baricco M and Enzo S 1980 *Philos. Mag.* **B61** 473
Eckert J, Schultz L and Urban K 1991 *Mater. Sci. Engg.* **A133** 393
Egami T and Waseda Y 1984 *J. Non-Cryst. Solids* **64** 113
El-Eskandarany M S, Itoh F, Aoki K and Suzuki R 1990 *J. Non-Cryst. Solids* **117/118** 729
Eshelby J D 1956 *Solid State Phys.* **3** 79
Fecht H J, Han G, Fu Z and Johnson W L 1990 *J. Appl. Phys.* **67** 1744
Friedel J 1964 *Dislocations* (Oxford: Pergamon) p. 418
Gallego L J, Somoga J A and Alonso J A 1990 *J. Phys. Condensed Matter* **2** 6245
Gilman P S and Benjamin J S 1983 *Ann. Rev. Mater. Sci.* **13** 279
Guo W, Martelli S, Burgio N, Magini M, Padella F, Paradiso E and Soletta I 1991 *J. Mater. Sci.* **26** 6190
Highmore R J, Evetts J E, Greer A L and Somekh R E 1987 *Appl. Phys. Lett.* **50** 566
Hori S, Tai H and Narita Y 1985 *Proc. rapidly quenched metals V*, (eds) S Steeb and H Warlimont (Amsterdam: Elsevier) pp 911
Johnson W L 1986 *Prog. Mater. Sci.* **30** 81
Koch C C 1989 *Ann. Rev. Mater. Sci.* **19** 121
Koch C C, Cavin O B, Mc Kamey C G and Scorbrough J O 1983 *Appl. Phys. Lett.* **43** 1017
Lee P Y and Koch C C 1987 *J. Non-Cryst. Solids* **94** 88
Lee P Y, Jang J and Koch C C 1988 *J. Less Common Metals* **140** 73
Massalski T B and Woychik C G 1985 *Acta Metall.* **33** 1873
Matsuki K, Inoue A, Kimura H M and Masumoto T 1988 *Mater. Sci. Engg.* **97** 47
Miedema A R, de Chatel P F and de Boer F R 1980 *Physica* **B100** 1
Murray J L 1988 *Metall. Trans.* **A19** 243
Murty B S, Ranganathan S and Mohan Rao M 1989 *Proc. of the Indo-US workshop on metastable microstructures, Goa* (in press)
Murty B S, Mohan Rao M and Ranganathan S 1990 *Scr. Metall.* **24** 1819
Murty B S, Ranganathan S and Mohan Rao M 1992 *Mater. Sci. Engg.* **A149** 231
Niessen A K, de Boer F R, Boom R, de Chattel P F, Mattena W C H and Miedema A R 1983 *Calphad* 7 52
Oehring M and Bormann R 1991 *Mater. Sci. Engg.* **A134** 1330
Pearson W B 1974 *Handbook of lattice spacings and structures of metals and alloys*, (Oxford: Pergamon)
Politis C and Johnson W L 1986 *J. Appl. Phys.* **60** 1147
Schultz L 1988 *Mater. Sci. Engg.* **97** 15
Schulz R, Trudeau M L and Van Neste A 1991 *Mater. Sci. Engg.* **A134** 1354
Schwarz R B and Johnson W L 1983 *Phys. Rev. Lett.* **51** 415
Schwarz R B and Koch C C 1986 *Appl. Phys. Lett.* **49** 146
Schwarz R B, Petrich R R and Saw C K 1985 *J. Non-Cryst. Solids* **76** 281
Schwarz R B, Nash P and Turnbull D 1987 *J. Mater. Res.* **2** 456
Simozar S and Alonso J A 1984 *Phys. Status Solidi* **A81** 55
Smithells C J 1983 *Metals reference book* (London: Buttersworth) p. 13–10 13- 56
Sundaresan R and Froes F H 1987 *J. Metals* **39** 22
Sundaresan R, Jackson A G, Krishna Murthy S and Froes F H 1988 *Mater. Sci. Engg.* **97** 115
Suryanarayana C and Froes F H 1991 *Proc. INCAL-91* (eds) E S Dwarakadasa, S Seshan and K P Abraham, p. 593
Uenishi K, Kobayashi K F, Ishihara K N and Shingu P M 1991 *Mater. Sci. Engg.* **A134** 1342
Van der Kolk C J, Miedema A R and Niessen A K 1988 *J. Less Common Metals* **145** 1
Veltl G, Scholz B and Kunze H D 1991 *Mater. Sci. Engg.* **A134** 987
Weeber A W 1987 *J. Phys. F: Met. Phys.* **17** 809
Weeber A W and Bakker H 1988 *Physica* **B153** 93
Willey L A and Margolin H 1973 *Metals Handbook* (Metals Park, Ohio: ASM) p. 264